Characteristics of Air Bubble Rising in Low Concentration Polymer Solutions

*HASSAN, N. M. S., KHAN, M. M. K. AND RASUL, M. G.

College of Engineering and Built Environment
Faculty of Sciences, Engineering and Health
Central Queensland University
Rockhampton, Qld-4702
AUSTRALIA
*n.hassan@cqu.edu.au

Abstract: - The bubble rise phenomena in different low concentration polymer solutions for higher Reynolds number are presented in this paper. The main characteristics, namely, the bubble velocity, the bubble trajectory and the drag relationship are investigated. The experiments were conducted in two different cylindrical columns at various liquid heights by introducing different bubble volumes (from 0.1mL to 20.0mL) corresponding to each height. The bubble rise velocity, bubble size and bubble trajectory were measured using a combination of non-intrusive-high speed photographic method and digital image processing. The parameters that significantly affect the rise of air bubble are identified. The bubble rise velocity of different volumes and the effect of liquid heights on the bubble rise velocity are analysed and discussed. The results show that the average bubble rise velocity increases with the increase in bubble volume for different low concentration polymer solutions and the bubble velocity is not dependant on the size of the test rig. The results of bubble trajectory for various bubbles are compared and discussed. In trajectory analysis, it is seen that the smaller bubbles show helical or zigzag motion and larger bubbles follow spiral motion. A new set of data of the drag coefficient for air bubble for higher Reynolds number are reported and compared with the results of other analytical and experimental studies available in the literature. The bubble rise characteristics, i.e., bubble velocity, trajectory and drag coefficient produced acceptable and consistent results.

Key-words: - Bubble rise velocity, bubble trajectory, bubble volume, drag co-efficient, Reynolds number, polymer solution, non-intrusive method

1 Introduction

Air bubbles are used in chemical, biochemical, environmental, and food process for improving the heat and mass transfer. Bubbles play an important role in many applications such as; in the fermentation process, in the cooking processes, in determining the rates of heat and mass transfer and coalescence, in the pipeline transport applications, in polymer and sludge processes and others [1]. The bubbles find uses in many process industries such as in vacuum pan operation in sugar industries which is an important process for the production of raw sugar.

The most significant dynamic behaviour of air bubbles are the bubble rise velocity, trajectory and the drag coefficient. The drag coefficient correlates the drag force exerted on a moving air bubble to its terminal velocity and projected surface area. The terminal velocity of an air bubble is termed as the velocity attained at steady state conditions where all applied forces are balanced. When the bubble rises in a liquid column, buoyancy and drag forces govern the rise velocity of the bubble. Drag and buoyancy forces are strongly dependent on fluid properties, gravity and the equivalent diameter of the bubble. The bubble rise velocity and drag coefficient of an air bubble are mainly dependent on the properties of the liquid and the bubble. For low-Reynolds number flows, the viscous forces are large relative to internal terms and the viscous shear stresses transmit the motion of the bubble far into the flow. So the viscosity forces dominate the terminal motion and terminal rise velocity increases with diameter of the bubble at very low Reynolds number. An intermediate region (Re>1), bubbles are no more spherical as their size increases and terminal velocity may increase or remain constant or decrease with equivalent diameter of the bubble. In this region, surface tension and inertia forces determine the

terminal rise velocity. On the other hand, in very high Reynolds number flows the viscous shear stresses only affect the flow close to the wall so a thin boundary layer forms near the bubble where the velocity varies from a finite value (relative velocity between the bubble and medium) to approximately zero. The flow outside of this layer is caused by the pressure gradients. The adverse pressure gradient formed as the flow moves around the back of the bubble causes the flow to separate from the bubble. The location of this flow separation and the nature of the separation (either steady or unsteady) are calculated by the interaction between the pressure gradients outside the boundary layer and the viscous flow near the bubble so it is determined by the Reynolds number of the flow. At high Reynolds number, bubbles are spherical cap or mushroom shaped and the motion of the bubble is dominated by the inertia forces. In this region, bubble rise velocity increases with the equivalent diameter of the bubble [2].

Bubble rise characteristic in Newtonian liquid has received considerable attention and is well studied. Due to the dominance of non-Newtonian liquids used in various process industries, an understanding of bubble rise in rheologically complex liquids has grown to be important. The dynamics of the bubble characteristics in a gas-liquid system are still not totally understood. From most of the study, it was seen that a small bubble rises through water in a straight line at its terminal velocity until it finishes its journey. The paths of larger bubbles were not stable and started to zigzag and much larger bubbles followed spiral motion [3 -8]. Shew and Pinton [5] presented that the shift of the onset of path instability to smaller bubble size changes remarkably in the case of polymer solution and it also appeared that the bifurcation to path instability for increasing bubble size was less abrupt for the polymer solution in comparison with water.

Dewsbury et al. [9] have investigated the relationship between the terminal velocity and volume for larger gas bubbles in non-Newtonian power-law fluids. Tsuge and Hibino [10] reported that the trajectories of rising spherical and ellipsoidal gas bubbles at higher Reynolds numbers are identical. Dewsbury et al. [11] determined experimentally that the drag coefficient for a rising solid sphere in non-Newtonian pseudo plastic liquids were significantly affected by its trajectory. A new drag correlation for rising spheres in power-law liquids was presented by Dewsbury et al. [12]. It is valid for $0.1<Re<25000$. It described the relationship between C_d and Re in creeping, transitional, turbulent and even critical flow regimes. Margaritis et al. [13] studied the drag co-efficient variation for bubbles over a wide range of Re in different non-Newtonian polysaccharide solutions and proposed a correlation which matched very well with experimental data. For the case of power-law non-Newtonian fluids, it has been shown that the drag curve for air bubbles followed Hadamard-Rybczynski model rather than Stokes model for $Re < 5$ [11, 14]. On the other hand, Miyahara and Yamanaka [14] reported for the case of highly viscous non-Newtonian liquid that the drag coefficient deviates from the Hadamard – Rybczynski type equation if the Reynolds number increases. Dhole et al. [15] investigated that the drag co-efficient always increases with the increase in power law index for all values of the Reynolds number.

There have been limited studies available in the literature on bubble rise characteristics in low concentration polymer solutions at high Reynolds number. More research and in–depth analysis on bubble rise phenomena in non-Newtonian fluid is necessary as most of the industrial fluids are non-Newtonian in nature. The aim of this study is to measure the bubble rise velocity, bubble trajectory, and the drag on the bubble as it rises through low concentration polymer (shear thinning) fluids and investigate the influence of various parameters namely, the bubble sizes, fluid properties on the bubble rise characteristics (velocity, trajectory, drag etc).The correlation of drag co-efficient of the bubble at a higher Reynolds number is compared with the results of other analytical and experimental studies available in the literature.

2 Experimental Set-up and Procedure

2.1 Experimental test rig

The experimental set up selected in this study was similar to that used by Dewsbury et al. [9]. The experimental apparatus is shown schematically in Fig. 1. Two-test rigs were used for investigating the bubble rise characteristics in xanthan gum and polyacrylamide solution. The first rig consisted of a polycarbonate tube approximately 1.8 m in height and 125 mm in diameter. The bubble insertion mechanism consisted of a ladle or spoon that had a capability to control the injection of air. The second rig was designed with acrylic tube of 400 mm in diameter and 2.0 m in height. Larger sizes of bubble were tested in this rig to eliminate the wall effect. The camera lifting apparatus stands approximately 2.0 m high which allows the movement of the camera mount device to rise through 1.8 m in height. The variable speed drive of camera lifting apparatus regulates the control of the camera

mount device. This drive allows the camera to be raised at approximately the same velocity as the bubble. A high speed digital video camera (Panasonic, NV-GS11, 24X optical Zoom) was mounted on a camera mount device with a small attachment to the side of the camera lifting apparatus.

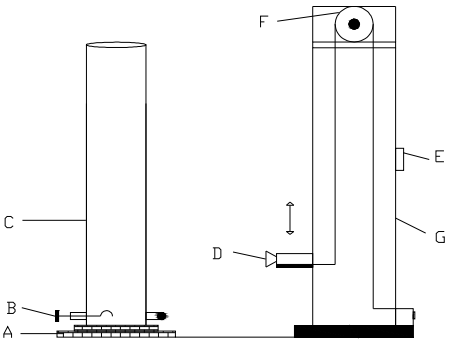

A = Sturdy Base; B = Rotating Spoon; C = Cylindrical test rig (0.125m or 0.40 m diameter), D = Video camera; E = Variable speed motor; F = Pulley; and G = Camera lifting apparatus.

Fig. 1 Schematic diagram of experimental apparatus

2.2 Bubble rise velocity measurement

Bubble rise velocities were computed by a frame by frame analysis of successive images. The bubble images were analysed with the software "Windows Movie Maker" by which the bubble rise time was recorded and velocity was measured. It is noted that the bubble velocity was measured at different liquid heights of 1 m, 1.2 m, 1.4 m and 1.6 for both xanthan gum and polyacrylamide solutions.

2.3 Bubble diameter measurement

Bubble equivalent diameter was measured from the still frames which were obtained from the video image. The still images were then opened using "SigmaScan Pro 5.0" commercial software and the bubble height (d_h) and the bubble width (d_w) were measured in pixels. The pixel measurements were converted to millimetres based on calibration data for the camera. The bubble equivalent diameter, d_{eq} was calculated [16] as

$$d_{eq} = \left(d_h \times d_w{}^2\right)^{\frac{1}{3}} \tag{1}$$

where d_w the long axis length and d_h is the short axis length of the bubble. For this measurement it was assumed that the bubble was axi-symmetric with respect to its height or short axis direction.

2.4 Bubble trajectory measurement

Trajectory was determined from the still images collected from the digital video camera. Bubble trajectory was computed from the still frames obtained from the video image. The still frames were then opened in "SigmaScan Pro" commercial software, which was capable of showing pixel location on an image.

A bubble images that had been stored in the computer were opened in 'Adobe Photoshop' commercial software. The pixel coordinates (X and Y) of the bubbles centre were noted and recorded into spreadsheet. X coordinate corresponds the distance from the left edge and Y coordinate corresponds the distance from the top edge respectively. The pixel line running through the centre of the bubble release point was known. The deviation of the bubble centre from the release point was computed by subtracting the X of the bubble centre from the X of the bubble release point.

2.4 Calculation of Reynolds number and drag coefficient

Since the fluid viscosity changes as a function of the shear rate so the terminal velocity of the bubble also changes with the change in shear rate. The average shear rate over the entire bubble surface is equal to U_b/d_b so the apparent viscosity can be written [13, 17] as

$$\mu = K\left(U_b/d_b\right)^{n-1} \tag{2}$$

In the case of spherical bubble, the Reynolds number for non-Newtonian power law fluid was defined as

$$\mathrm{Re} = \frac{\rho_{liq} d_b^n U_b^{2-n}}{K} \tag{3}$$

For a non-spherical bubble with a vertical axis of symmetry, the Reynolds number was defined [3, 13, 17, 18] by

$$\mathrm{Re} = \frac{d_w^n U_b^{2-n} \rho_{liq}}{K} \tag{4}$$

The drag co-efficient for spherical bubble was calculated by

$$C_d = \frac{4 g d_b \Delta\rho}{3 \rho_{liq} U_b^2} \tag{5}$$

In the case of non-spherical bubble, the drag co-efficient was computed by

$$C_d = \frac{4 g d_{eq}^3 \Delta\rho}{3 \rho_{liq} d_w^2 U_b^2} \tag{6}$$

The drag co-efficient for non-spherical bubble was calculated on the basis of the real bubble geometry in

equation (6), where d_{eq} is the equivalent sphere diameter and d_w is the diameter of the horizontal projection of bubble or long axis length of the bubble.

2.5 Test fluids

The polymer solutions xanthan gum and polyacrylamide used in this study were a non-Newtonian (shear thinning) fluid. The solutions (polyacrylamide and xanthan gum) with concentration of 0.025% (by weight) were used. The fluids were prepared by mixing 0.025% by weight of each material with water in the test rig and stirring it for long hours (5 -7 hrs). The temperature of all solutions in this study was maintained at $25^{\circ}C$. For every solution, the measured density of the solution was very close to the density of water at $25^{\circ}C$ since they were low concentration liquids. Rheological properties of the solutions were measured using an ARES (Advanced Rheometric Expansion System) rheometer. The rheological properties for different solutions are summarized in Table 1. The usual range of shear rate to determine fluid rheology was 1 -650s^{-1}.

Table 1 Rheological and physical properties of polymer solutions

Fluid Type	Concentration (%)	K, $Pa.s^n$	n	Density, kg/m^3
Polyacrylamide	0.025	0.00502	0.8544	998.0
Xanthan Gum	0.025	0.00720	0.7975	999.02

Fig. 2 shows that the polymer (xanthan gum and polyacrylamide) solutions exhibit non-Newtonian shear-thinning pseudoplastic behaviour which is adequately described by Power-Law model,

$$\eta = K\dot{\gamma}^{n-1} \qquad (7)$$

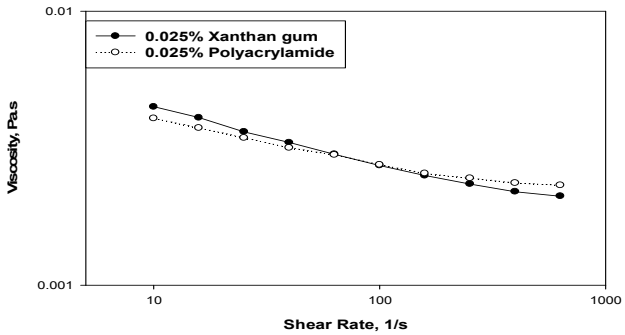

Fig. 2 Viscosity vs. shear rate of xanthan gum solutions demonstrating the pseudoplastic behaviour.

The K and n values for the polymer solutions were determined from this response curve and are shown in the Table 1. K represents the consistency of the fluid behaviour i.e. the higher the value of K, the more viscous the fluid and n denotes power law index which is a measure of the extent of non-Newtonian behaviour. As seen, the viscous effect of the xanthan gum solution was more than that of polyacrylamide solution because the value of K was found slightly higher.

3 Results and Discussion

3.1 Bubble rise velocity

The velocity profile of xanthan gum and polyacrylamide solutions for bubble volumes of 0.1mL- 5.0mL, carried out in the smaller rig (125 mm) at different liquid heights are presented in Fig. 3. It is seen that the bubble velocity increases with the increase in bubble volume for both solutions. The average bubble velocity for these bubble sizes was between 0.22 m/sec and 0.30 m/sec. The velocity profile of xanthan gum and polyacrylamide solutions for bubble volumes of 0.1mL- 20mL measured at different liquid heights in the larger test rig (400 mm) are shown in Fig. 4. It shows the same phenomena as observed in Fig. 3. The average bubble velocity for these bubble sizes was between 0.22 m/sec and 0.41 m/sec at 1.0 m height. As seen, the velocities for corresponding bubble sizes are nearly same for both solutions. However, for the bubble volume of 20mL at a height of 1 m, the bubble velocity of xanthan gum is found slightly lower than that of polyacrylamide solution. This is due to the higher viscosity of xanthan gum as higher viscosity restrains the bubble to rise faster.

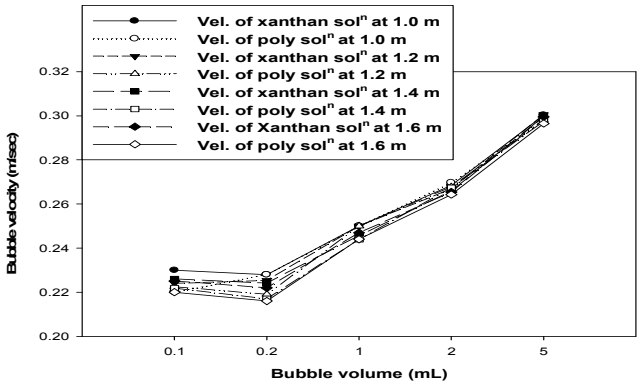

Fig. 3 Velocity profile for polyacrylamide and xanthan gum solutions at different heights (125mm rig)

It can be observed from Fig. 3 and Fig. 4 that the average bubble velocity slightly decreases with the increase in liquid height but not to a significant extent, although the pressure changes with the increase in height is very small.

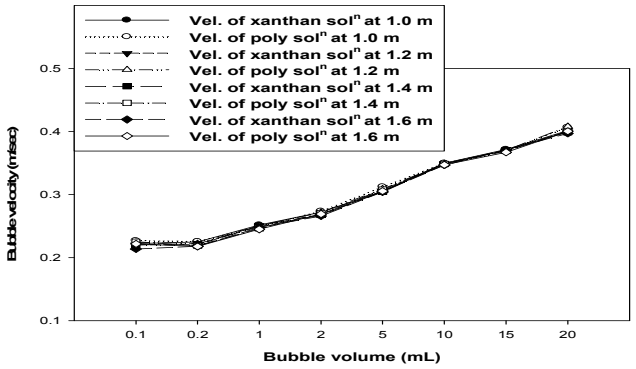

Fig. 4 Velocity profile for polyacrylamide and xanthan gum solutions at different heights (400mm rig).

Davies and Taylor [19] proposed in their study a correlation for the calculation of the bubble rise velocity which is shown in equation (8). The same (8) was also used by Talaia [20] for larger bubbles.

$$U_b = 0.707\sqrt{gd_{eq}} \qquad (8)$$

The current results of bubble rise velocity as a function of the bubble equivalent diameter is compared with the result of Davies and Taylor in Fig. 5. As seen, the current experimental data agrees well with this correlation for larger bubbles at higher Reynolds number with some variations for lower bubble size in low Reynolds number. This is consistent since the equation (8) is valid for larger bubbles.

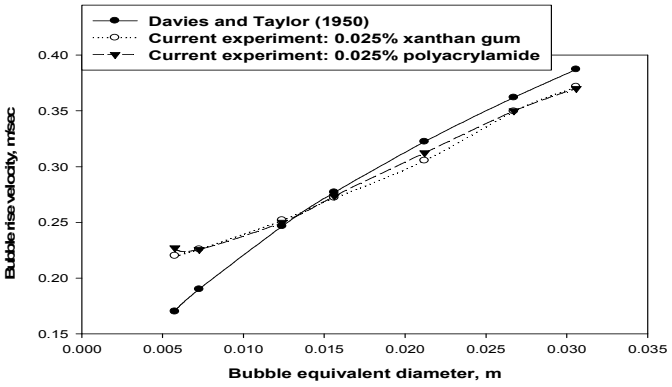

Fig. 5 Bubble rise velocity vs. bubble equivalent diameter

Fig. 6 presents the data obtained from both test rigs for a liquid column of 1.0 m height. It is seen that the bubble velocity data fall on the same straight line for corresponding bubble volume and liquid height. A similar trend was also found for all liquid heights. Hence the bubble velocity was found to be rig independent.

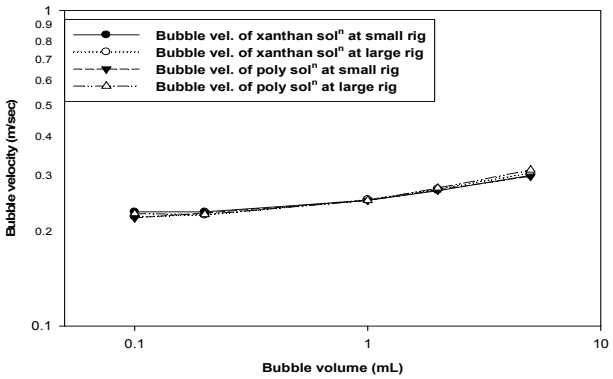

Fig. 6 Velocity profile at different rig size corresponds to the same bubble volume.

3.2 Bubble trajectory

The trajectory results of xanthan gum solution are shown in Fig. 7 for different bubble sizes when measured over a height of 1.0 m from the point of air injection. The figure shows the deviation of bubble from its release point as it rises through a liquid column. The general trend was for the bubble to remain close to the release centre, when the bubble was released and as it rose through the liquid, it spread out as the height increases.

For the xanthan gum solution, the smaller bubbles (0.1mL and 2mL) deviated more horizontally with respect to the bubble release centre and the bubble traveled with a helical motion. The larger bubble of 5.0mL initially deviated horizontally and finally, they followed a spiral path. In the beginning, the 10mL bubble followed the straight path, then deviated horizontally and finally followed spiral path. Smaller bubbles less than 2 mm in diameter rise in straight or linear path [21, 22] but the linear trajectory was not observed as the bubble equivalent diameter of this study was more than 5 mm. At low Re for smaller bubble, the rising bubble showed a zigzag trajectory. At high Re, the larger bubbles displayed a spiral trajectory because the effect of wake shedding influenced the bubble to induce a spiraling rising motion. The horizontal movement is observed less in polymer solution in the case of smaller bubbles than that of water where the small bubbles deviate more than the larger bubbles [6, 7, 23, 24].

In the xanthan gum solutions, the horizontal motion of the smaller bubble is reduced than that of water due to increase in viscosity and less friction acting upon their surface compared to the larger bubbles and so the smaller bubbles experience less resistance to vertical movement. The larger bubbles however experience more resistance on top and deform as their size increases that result in spiral motion.

Fig. 8 shows the trajectory results of polyacrylamide solution. It can be seen that the polyacrylamide solution shows the similar phenomena as is observed for xanthan gum solution in Fig. 7. However, the horizontal movement of smaller bubbles is observed a little bit less in comparison with xanthan gum solution due to less viscosity of polyacrylamide solution.

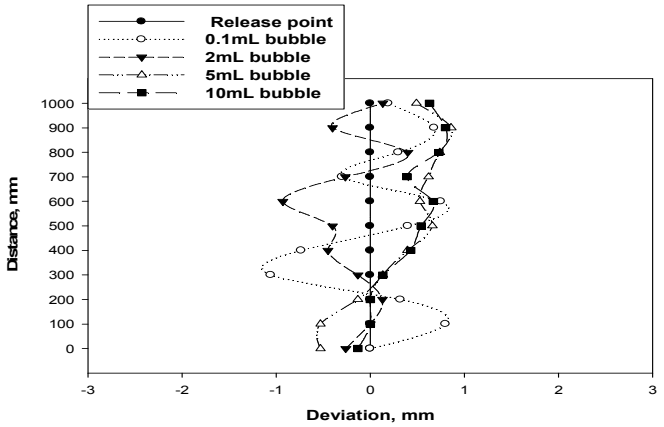

Fig. 7 Rise trajectories of different sizes of bubbles in 0.025% xanthan gum solution.

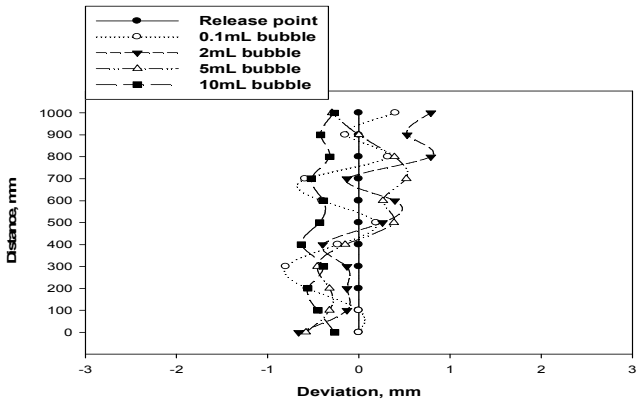

Fig. 8 Rise trajectories of different sizes of bubbles in 0.025% polyacrylamide solution.

3.3 Drag co-efficient

Bubble drag coefficients as a function of Reynolds number for xanthan gum and polyacrylamide solutions are presented in Fig. 9 and Fig. 10 respectively.

For $\mathrm{Re} \le 0.1$, the creeping flow regime, the governing equation for drag force can be given by [25],

$$F_d = 3\pi\mu d_b U_b \tag{9}$$

which is a form of Stokes Law. This Stokes model is given by

$$C_d = \frac{24}{\mathrm{Re}} \tag{10}$$

The equation (10) is only valid for solid bubble or particle at very low Reynolds number but not suitable for gas bubbles rising in power-law liquids. It is noted that no universal drag curve for the case of rising air bubbles in non-Newtonian Power-Law fluids has been developed yet in the available literature. The gas bubbles obey the Hadamard-Ryczynski model at very low Reynolds number which is given [14] by

$$C_d = \frac{16}{\mathrm{Re}} \tag{11}$$

The drag coefficient for solid particles can also be determined [26] by,

$$C_d = \frac{24}{\mathrm{Re}}\left(1+0.173\,\mathrm{Re}^{0.657}\right)+\frac{0.413}{1+16{,}300\,\mathrm{Re}^{-1.09}} \tag{12}$$

The above correlation converges to Stokes model at low Re number. A modified correlation was proposed for gas bubbles in non-Newtonian power-law fluids [3], given by

$$C_d = \frac{16}{\mathrm{Re}}\left(1+0.173\,\mathrm{Re}^{0.657}\right)+\frac{0.413}{1+16{,}300\,\mathrm{Re}^{-1.09}} \tag{13}$$

The equation (13) converges to the Hadamard - Rybczynski equation, at low Reynolds number.

The following two equations (14) and (15) have been suggested for spherical bubbles [21],

$$C_d = 0.28 + \frac{6}{\mathrm{Re}^{0.5}} + \frac{21}{\mathrm{Re}} \tag{14}$$

$$C_d = 0.2924\left(1+9.06\,\mathrm{Re}^{-0.5}\right)^2 \tag{15}$$

The above equations are valid for (0.1< Re< 4000) and (Re < 6000) respectively. Again, the equation (14) was also used by other researcher for spherical bubble [27].

It can be seen from Fig. 9 that the deviation of the experimental C_d was initially higher in comparison with the equations (12), (13), (14) and (15) but this deviation appeared to be less with the increase in Re. For Re = 3200 and higher, it is seen that the values of the experimental C_d and the predicted C_d from these equations are nearly same and constant. This phenomenon is also observed in Fig.10 for polyacrylamide solution at Re = 4000 and higher.

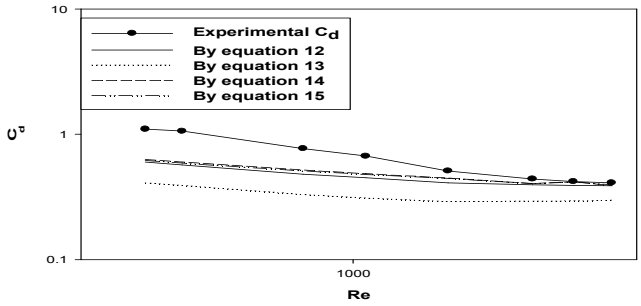

Fig. 9 Drag coefficients vs. Reynolds number for rising air bubble in xanthan gum solution.

.

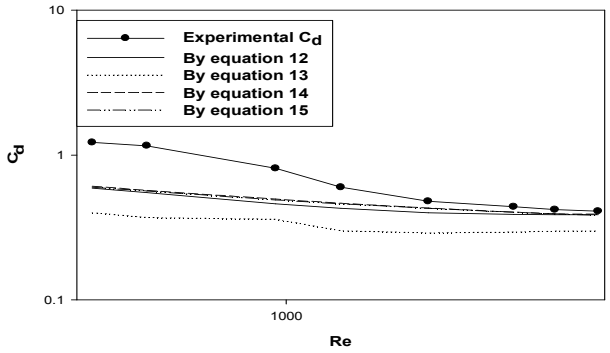

Fig. 10 Drag coefficients vs. Reynolds number for rising air bubble in polyacrylamide solution

The reported experimental data of drag coefficient constitute a new set of data for air bubble at higher Reynolds number beyond Reynolds number of 1000. As seen, these new data are described well with the published equations mentioned above.

5 Conclusions

The following conclusions can be reached from this study:

- The average bubble rise velocity increases with the increase in bubble volume for both xanthan gum and polyacrylamide solutions.
- The average bubble velocity slightly decreases with the increase in liquid height for corresponding bubble volume.
- The bubble velocity of xanthan gum is found slightly lower than the velocity in polyacrylamide solution for corresponding bubble sizes.
- The bubble velocity is not dependant on the size of the test rig.
- In the trajectory analysis, it is seen that small bubbles followed a helical motion while larger bubbles followed a spiral motion. As the bubble size increases, initially, the bubble follows straight path, attains its terminal velocity and shape, then it switches to spiral path.This is due to the increase in viscosity and less resistance on rising of bubbles.
- A new set of data of drag co-efficient are reported for higher Reynolds number beyond the Re = 1000.
- The relationship between C_d-Re for low concentration polymer solution showed acceptable results with the available analytical and experimental studies of the literature but it deserves further study for a wide range of Reynolds number.

Nomenclature:

d_b	[m]	bubble diameter
d_h	[m]	bubble height
d_w	[m]	projected diameter onto horizontal plane
d_{eq}	[m]	equivalent sphere diameter
μ	[Pa.s]	apparent viscosity
Re	[-]	Reynolds number
C_d	[-]	drag coefficient
F_d	[N]	drag force
g	[m/s^2]	acceleration due to gravity
U_b	[m/s]	bubble rise velocity
n	[-]	power law index
K	[Pa.s^n]	consistency index
g	[m/s^2]	gravitational acceleration
$\dot{\gamma}$	[s^{-1}]	shear rate

Greek letters

$\Delta\rho$	[kg/m^3]	density difference between liquid and air bubble
ρ_{liq}	[kg/m^3]	liquid density

References:

[1] Shosho, C. and Ryan, Micheal, E., An experimental study of the motion of long bubbles in inclined tubes, Chemical engineering science, 56, 2001, 2191-2204.

[2] Kulkarni, A. A. and Joshi, J. B., Bubble Formation and Bubble Rise Velocity in Gas-Liquid Systems: A

Review, Ind. Eng. Chem. Res., 44, 2005, 5873-5931.

[3] Shew, W. L., Poncet, S. and Pinton, J. F., Viscoelastic effects on the dynamics of a rising bubble, Journal of statistical Mechanics, P01009, 2006.

[4] Shew, W. L. and Pinton, J. F., Dynamical Model of Bubble path Instability, PRL 97, 144508, 2006.

[5] Wu, Mingming., Gharib, Morteza., Experimental Studies on the Shape and Path of Small Air Bubbles Rising in clean Water., Physics of Fluids, vol.14, no.7, 2002.

[6] Hassan, N. M. S., Khan, M. M. K. and Rasul, M. G., A Comparative Study of Bubble Rise Phenomena in Water and Low concentration Polymer Solutions, HEFAT 2007, Heat Transfer, Fluid Dynamics and Thermodynamics – 5th international Conference, Sun City, South Africa, July, 1-4, 2007.

[7] de Vries, A. W. G., Biesheuvel, A. and van Wijngaarden, L., Notes on the path and wake of a gas bubble rising in pure water, Int. J. Multiph. Flow 28, 1823, 2002.

[8] Mougin, G. and Magnaudet, J., Phys. Rev. Lett. 88, 014502, 2002.

[9] Dewsbury, K., Karamanev, D. G. and Margaritis, A., Hydrodynamic Characteristics of free Rise of Light solid Particles and Gas Bubbles in Non-Newtonian Liquids., Chemical engineering Science, vol. 54, 1999, pp.4825-4830.

[10] Tsuge, H., and Hibino, S., The motion of Single Gas Bubbles Rising in Various Liquids., Kagaku Kogaku, 35, 65, 1971.

[11] Dewsbury, K., Karamanev, D .G. and Margaritis, A., Dynamic Behavior of Freely Rising Buoyant Solid Spheres in Non-Newtonian Liquids, AIChE Journal, Vol. 46, No. 1, 2000.

[12] Dewsbury, K., Karamanev, D. G. and Margaritis, A., Rising solid sphere hydrodynamics at high Reynolds numbers in non-Newtonian fluids, Chemical Engineering Journal, 87, 2002, 129-133.

[13] Margaritis A., te Bokkel, D. W. and Karamanev, D. G., Bubble Rise Velocities and Drag Coefficients in non-Newtonian Polysaccharide solutions, John Wiley & Sons, Inc., 1999.

[14] Miyahara, T. and Yamanaka, S., Mechanics of Motion and Deformation of a single Bubble Rising through Quiescent Highly Viscous Newtonian and non-Newtonian Media, Journal of chemical engineering, Japan, Vol. 26, No. 3, 1993.

[15] Dhole, S. D., Chhabra, R. P. and Eswaran, V., Drag of a Spherical Bubble Rising in Power Law Fluids at Intermediate Reynolds Numbers., Ind. Eng. Chem. Res. 46, 2007, 939 – 946.

[16] Lima-Ochoterena, R. and Zenit, Visualization of the flow around a bubble moving in a low viscosity liquid, Revista Mexicana De Fisica 49 (4), 2003, 348 – 352.

[17] Lali, A. M., Khare, A. S., Joshi, J. B. and Nigam, K. D. P., Behaviour of Solid Particles in viscous Non-Newtonian Solutions: Settling Velocity, Wall Effects and Bed Expansion in Solid-Liquid Fluidized Beds, Powder Technology, 57, 1989, 39 – 50.

[18] Miyhara, T. and Takahashi, T., Drag coefficient of a single bubble rising through a quiescent liquid., International Chemical Engineering, Vol. 25, No. 1, 1985.

[19] Davies, R. M. and Taylor, G. I., The mechanics of large bubbles rising through liquids in tubes, Proc. of Roy. Soc., London, 200, Ser. A, 1950, 375 – 390.

[20] Talaia, Mario A. R., Terminal Velocity of a Bubble Rise in a Liquid Column, International Journal of Applied Science, Engineering and Technology, Vol. 4, No. 3, 2007, ISSN 1307 – 4318.

[21] Clift, R., Grace, J. R and Weber, M. E., Bubbles, Drops and Particles; Academic Press, 1978, republished by Dover, 2005.

[22] Duineveld, P. C., The Rise Velocity and Shape of Bubbles in pure water at high Reynolds Number, J. Fluid Mech. vol. 292, 1995, 325-332.

[23] Hassan, N. M. S., Khan, M. M. K., Rasul, M. G. and Rackemann, D.W., An Experimental Study of Bubble Rise Characteristics in non – Newtonian (Power-Law) Fluids,16th Australasian Fluid Mechanics Conference, Crown Plaza, Gold Coast, Australia, 2-7 December, 2007.

[24] Krishna, R., van Baten, J.M., Rise Characteristics of Gas Bubbles in a 2D Rectangular Column: VOF Simulations vs. Experiments, Int. Comm. Heat Mass Transfer, vol. 26, no. 7, 1999, 965-974.

[25] Chhabra, R. P., Bubbles, Drops, and Particles in Non-Newtonian Fluids, Taylor & Francis Group CRC Press, 2006.

[26] Turton, R., and Levenspiel, O., A short note on the drag correlation for spheres, Powder Technology, 4, 1986.

[27] Zhang, Y. and Reese, J. M., The drag force in two-fluid models of gas–solid flows, chemical Engineering Science 58, 2003, 1641-1644.